

Article

## Second-Order Harmonic Reduction Technique for Photovoltaic Power Conditioning Systems Using a Proportional-Resonant Controller

Hae-Gwang Jeong, Gwang-Seob Kim and Kyo-Beum Lee \*

Department of Electrical and Computer Engineering, Ajou University, San 5, Woncheon-dong, Yeongtong-gu, Suwon 443-749, Kyunggi-do, Korea; E-Mails: lite88@ajou.ac.kr (H.-G.J.); bhj8@ajou.ac.kr (G.-S.K.)

\* Author to whom correspondence should be addressed; E-Mail: kyl@ajou.ac.kr;  
Tel.: +82-31-219-2376; Fax: +82-31-212-9531.

Received: 17 November 2012; in revised form: 6 December 2012 / Accepted: 17 December 2012 /  
Published: 02 January 2013

---

**Abstract:** This paper proposes a second-order harmonic reduction technique using a proportional-resonant (PR) controller for a photovoltaic (PV) power conditioning system (PCS). In a grid-connected single-phase system, inverters create a second-order harmonic at twice the fundamental frequency. A ripple component unsettles the operating points of the PV array and deteriorates the operation of the maximum power point tracking (MPPT) technique. The second-order harmonic component in PV PCS is analyzed using an equivalent circuit of the DC/DC converter and the DC/AC inverter. A new feed-forward compensation technique using a PR controller for ripple reduction is proposed. The proposed algorithm is advantageous in that additional devices are not required and complex calculations are unnecessary. Therefore, this method is cost-effective and simple to implement. The proposed feed-forward compensation technique is verified by simulation and experimental results.

**Keywords:** second-order harmonic; photovoltaic power conditioning system (PCS); single-phase inverter; proportional-resonant (PR) controller; ripple reduction

---

## 1. Introduction

Recently, the popularity of PV power generation systems has been growing exponentially [1]. However, owing to various environmental conditions, the controllability of input power is an important issue to be considered when PV systems are connected to the grid. Because of the penetration of renewable energy generation systems, power quality has become a popular research topic. A grid-connected PV PCS should satisfy grid standards such as flicker, frequency, and harmonics [2,3].

Power electronic devices and nonlinear loads have been used recently in the power grid; however, they introduce problematic harmonics into the system. The presence of harmonics in the power grid is harmful, because it will cause additional power losses, power quality degradation, reduction of equipment life, and component malfunctions. Therefore, international organizations such as the Institute of Electrical and Electronics Engineers (IEEE) and the International Electrotechnical Commission (IEC) have imposed harmonic control standards [2,3].

In order to compensate for harmonics in the system, passive power filters (PPFs) or active power filters (APFs) are used. In a particular frequency range, PPFs have low impedance and absorb harmonic currents. However, they have several disadvantages, such as detuning, resonance, instability, and limitations of the possible frequency adjustment [4,5]. The desired voltage and current can be obtained by a APF if the inverter circuit utilizes switch devices [6]. The APF generates a compensation current that has the opposite phase of a harmonic current. However, because of a high operation cost, extra hardware, and a complex control, the APF is not a superior solution [7].

Unlike PPFs and APFs, digital algorithms using a calculated ripple current compensation method [8] and a dual-loop control method [9] do not increase cost or volume. However, a calculated ripple current compensation method can be compensated the second-order harmonic without complex calculations. However, due to changes in parameters under various conditions, it is difficult to completely eliminate the second-order harmonic. In case of a dual-loop control method, large overshoots or undershoots can occur because of very low bandwidth settings.

An alternative solution is to use a PR controller. Owing to an infinite gain at the resonance frequency, the PR controller can achieve high performance in both the elimination of steady-state error in the stationary frame and the minimization of the load current distortion [10]. Because of these characteristics, the PR controller is easily used for eliminating the harmonic component in a selective harmonic compensator [1]. Therefore, the PR controller acts as a digital filter around the resonant frequency, without the need for additional devices. Considering the obvious advantages of PR controllers, they show promise for becoming a superior solution in place of APFs and PPFs.

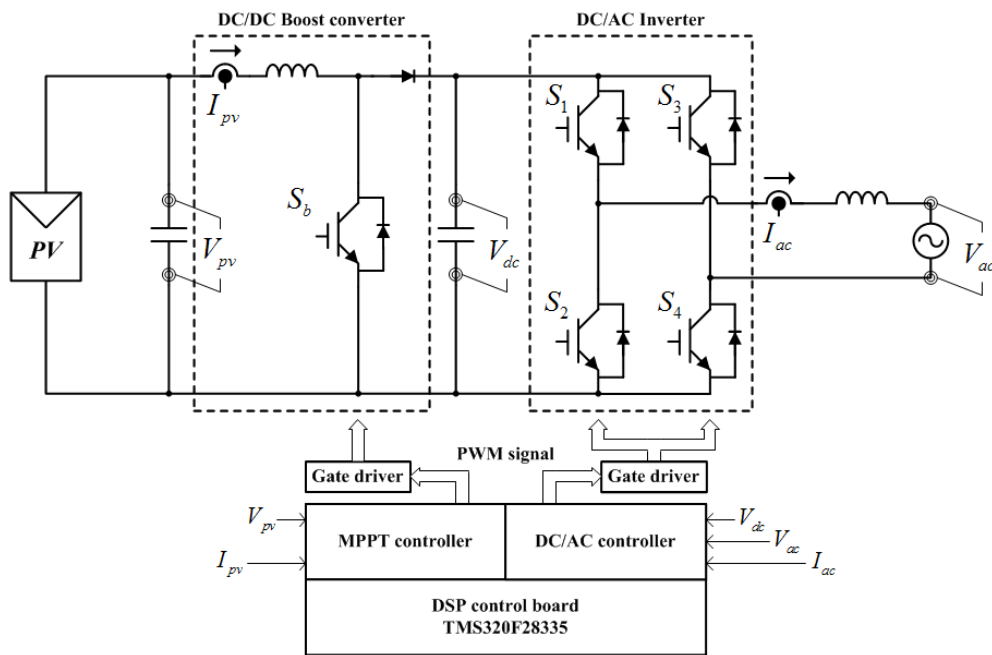
A grid-connected PV PCS typically consists of a converter and inverter. The converter is used to implement MPPT control and the inverter is used to control current for the unity power factor and a DC-link voltage control. In single-phase systems, a second-order harmonic component occurs systematically [8]. Such a ripple component perturbs the operating points of the PV array and degrades the performance of the MPPT control [11]. In the converter, the output current tracks the current command by using a proportional-integral (PI) current controller. A feed-forward compensation technique is implemented to eliminate the second-order harmonic component in the PV current. Since a compensated current consists of only a DC component, it is possible to perform an improved MPPT

control. A PSIM simulation and an experiment using a PV PCS are performed to verify the effectiveness of the proposed algorithm.

## 2. Description of Single-Phase PV PCS

Figure 1 shows a two-stage single-phase PV PCS that is commonly used. The PV PCS is composed of a PV array, DC/DC boost converter, DC-link, inverter, and inductor filter. To extract the maximum power from the PV array, the DC/DC boost converter has to perform MPPT control. In the DC/AC inverter, current control and DC-link voltage control are performed to deliver the generated power.

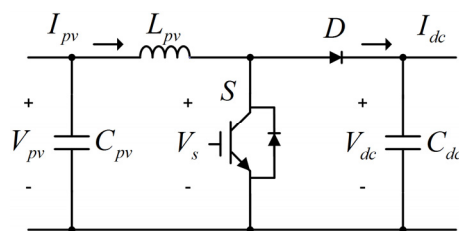
**Figure 1.** Diagram of a two-stage single-phase PV PCS.



### 2.1. DC/DC Boost Converter

The boost converter circuit (Figure 2) consists of a switch, diode, inductor, and capacitor. The switch  $S$  is controlled by a gating signal of a current controller.

**Figure 2.** DC/DC boost converter.



When the switch  $S$  is turned on, the voltage across the switch,  $v_s$ , is zero during on-time  $DT$ . Therefore, the inductor voltage  $v_L$  is approximately equal to the input voltage  $v_{pv}$  and the diode voltage  $v_D$  is equal to the output voltage  $v_{dc}$ .

When  $S$  is turned off, the voltage across the switch,  $v_s$ , is equal to the output voltage  $v_o$  and the diode voltage  $v_D$  is zero during off-time  $(1 - D)T$ . Hence, the inductor voltage  $v_L$  is equal to  $v_{pv} - v_{dc}$ . The inductor average voltage is given as:

$$V_L = V_{pv}D + (V_{pv} - V_{dc})(1 - D) \tag{1}$$

where  $D$  is the duty ratio of the switch  $S$ .

Because the inductor average voltage is zero in a steady state, the voltage transfer ratio  $G_v$  is:

$$G_v = \frac{V_{dc}}{V_{pv}} = \frac{1}{1 - D} \tag{2}$$

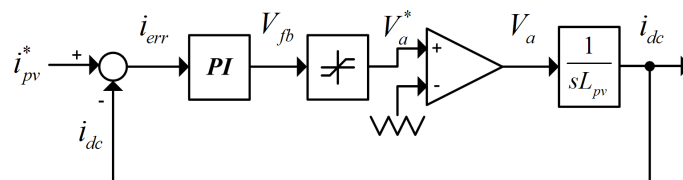
Because the duty ratio  $D$  is between 0 and 1, the output voltage must always be higher than the input voltage.

Figure 3 shows a conventional PI current controller scheme for a DC/DC boost converter. The current controller compares the inductor current  $i_{dc}$  and a reference current  $i_{pv}^*$  from the MPPT function. As depicted in Figure 4, the transfer function is derived as:

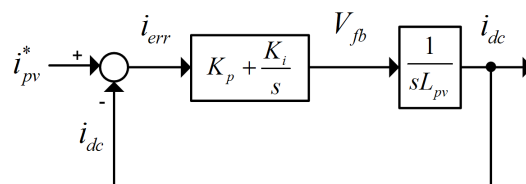
$$\frac{I_{dc}}{I_{pv}^*} = \frac{K_p s + K_i}{L_{pv} s^2 + K_p s + K_i} \tag{3}$$

where  $K_p$  and  $K_i$  are gain constants.

**Figure 3.** Conventional PI current controller.



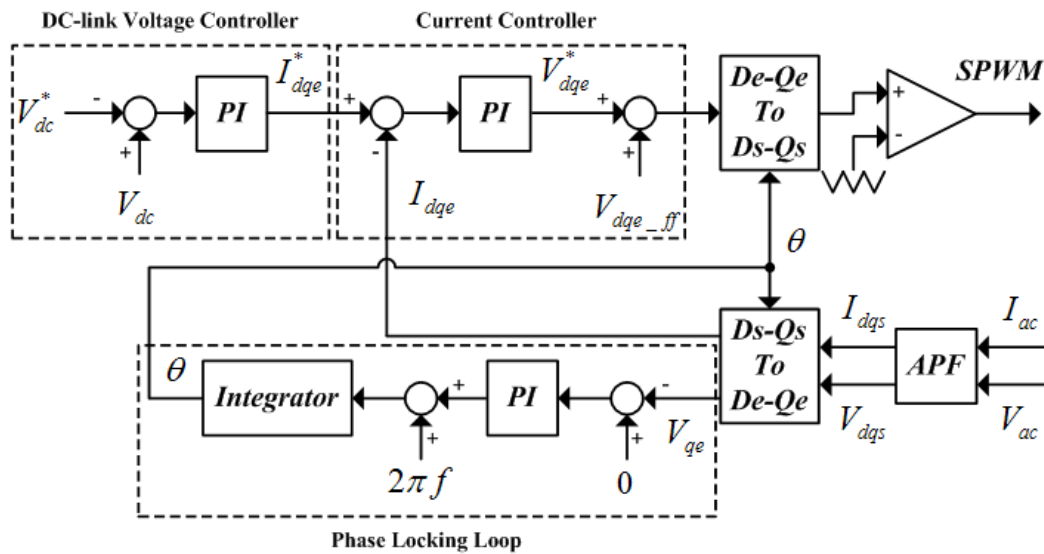
**Figure 4.** Simplified PI current controller.



### 2.2. DC/AC Inverter

Figure 5 shows a block diagram of DC/AC inverter control for single-phase system. In the phase-locking loop (PLL) for the grid synchronization, the estimated grid angle is used for the D-Q transformation. A grid voltage and current are converted to active and reactive component using the D-Q transformation and the APF. The DC/AC inverter converts DC power into AC power. As seen from Figure 5, the DC-link voltage controller and current controller is performed for unity power factor. As the DC-link voltage is higher than the reference DC-link voltage, the DC-link voltage controller increases the reference grid current and the output power is increased. In the contrary case, the DC-link voltage controller decreases the reference grid current and the output power is decreased.

Figure 5. Block diagram of DC/AC inverter control for single-phase system.



2.3. Analysis of Second-Order Harmonic

Figure 1 shows the two-stage single-phase PV PCS. The power equations for the PV-side and grid-side are:

$$PV\text{-side: } P_{pv} = V_{pv} I_{pv} \tag{4}$$

$$Grid\text{-side : } P_{ac} = V_{ac} I_{ac} = (V \cos \omega t)(I \cos \omega t) = VI \cos^2 \omega t = \frac{VI(1 + \cos 2\omega t)}{2} = \frac{VI}{2} + \frac{VI}{2} \cos 2\omega t \tag{5}$$

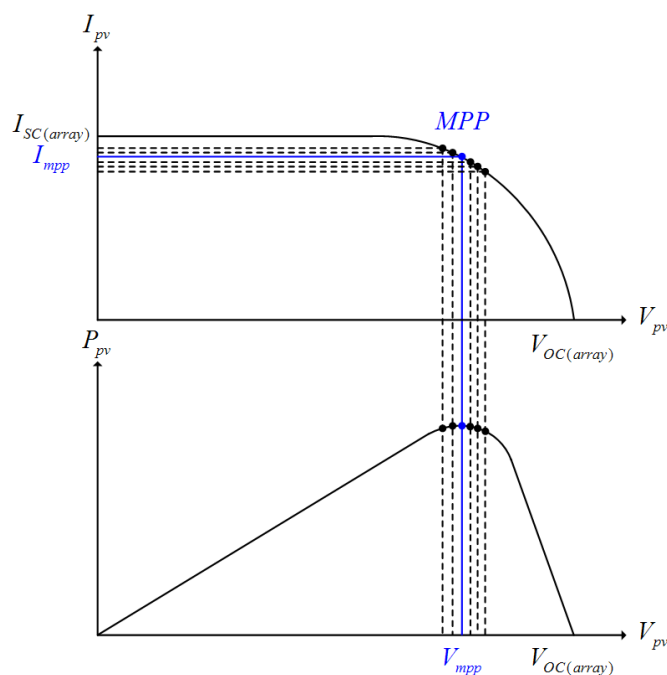
where  $\omega$  ( $= 2\pi f$ ) is the grid frequency.

If the input power and output power are equal, the input current ( $I_{pv}$ ) of a DC/DC boost converter can be calculated as [8]:

$$I_{pv} = \frac{V_{ac} I_{ac}}{V_{pv}} = \frac{VI}{2V_{pv}} + \frac{VI}{2V_{pv}} \cos 2\omega t \tag{6}$$

Equation (6) shows that  $I_{pv}$  is pulsating with the output power. The input current has a second-order harmonic at twice the fundamental frequency. Similarly,  $I_{dc}$  is pulsating with the output power in the DC-link. This means that the output current ( $I_{dc}$ ) of the DC/DC boost converter also has a ripple component. If the input current has no ripple components, the operating points are fixed as shown in Figure 6 (solid line).

However, if the input current has the ripple component, the operating points are continuously moving around a maximum power point (MPP). Therefore, the MPPT efficiency is reduced by ripples and noise [12].

**Figure 6.** Operating point of the PV array.

### 3. Proposed Second-Order Harmonic Reduction Technique

As mentioned above, the second-order harmonic inevitably occurs in single-phase systems. In [13], the use of a large bank of energy storage capacitors has been suggested. This method can reduce the ripple component, but it causes the entire system to be expensive and bulky. An active power filter was proposed, but this method also needs extra hardware and a complex control system [14].

In order to remove the harmonic, a ripple component can be calculated by manipulating system parameters [8]. The calculated second-order harmonic component is added to the output of controller for the feed-forward compensation. This method can be compensated the second-order harmonic without complex calculations. However, due to changes in parameters under various conditions, the calculated second-order harmonic component is inaccurate. Therefore, the 120 Hz ripple component cannot be removed completely.

A dual-loop control method is implemented in order to reduce the second-order ripple component [9]. In this method, a current controller is added to the existing DC-link voltage controller. In this case, the voltage loop bandwidth has to be set very low to reduce the second-order harmonic usually from 1 to 5 Hz. Owing to the lower voltage loop bandwidth, a large overshoot and undershoot of the DC-link voltage can occur during the transient-state.

#### 3.1. PR Controller

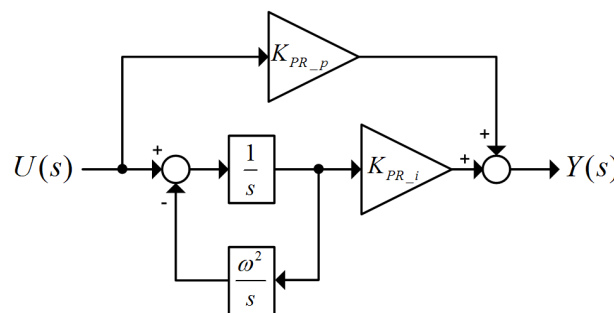
The PR controller is used in the stationary frame unlike the PI controller. The computation sequence of the PR controller is not complex because there is no transformation from the stationary frame to synchronous frame. For these reasons, a low-cost processor can be used. In addition, when grid unbalance or a sensing error occurs, the PR controller is more robust than the PI controller. Especially, the PR controller is suitable for constant frequency operation in the grid-connected system.

Generally, the PI controller has drawbacks such as difficulty in removing the steady-state error in a stationary reference frame. The PR controller structure recently gained considerable popularity owing to its capability of eliminating steady-state error when regulating sinusoidal signals [15–17]. Moreover, the easy implementation of a harmonic compensator without any adverse effect on the controller performance makes this controller well suited for grid-tied systems [18]. Figure 7 shows a block diagram of PR controller. The transfer function of the PR controller is defined below:

$$G_{PR}(s) = \frac{Y(s)}{U(s)} = K_{PR\_p} + K_{PR\_i} \frac{s}{s^2 + \omega^2} \tag{7}$$

where  $K_{PR\_p}$  and  $K_{PR\_i}$  are gain constants and  $\omega$  ( $= 2\pi f$ ) is the grid frequency.

Figure 7. PR controller.

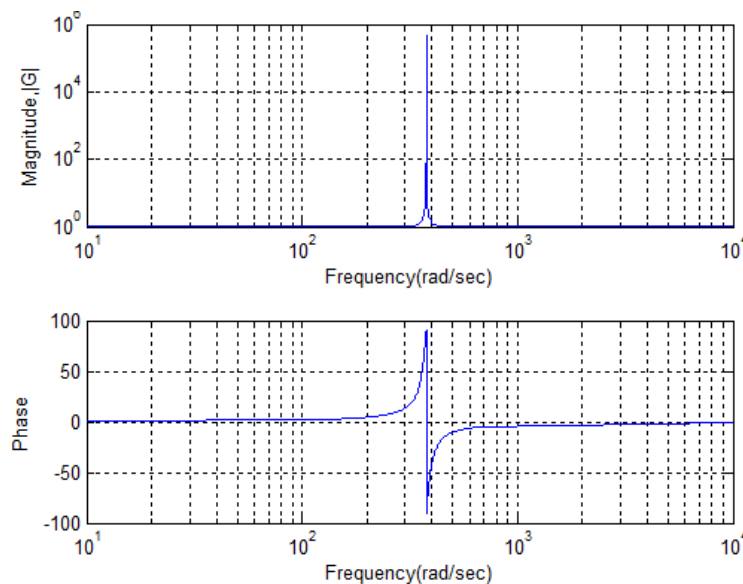


In Figure 8, the PR controller shows a very high gain and a zero phase shift at the frequency  $\omega$ . To avoid a stability problem associated with infinite gain, an approximating (non-ideal) PR controller using a high-gain low-pass filter is used [19]. The non-ideal PR controller can be expressed as:

$$G_{PR}(s) = K_{PR\_p} + K_{PR\_i} \frac{\omega_c s + \omega_c^2}{s^2 + 2\omega_c s + \omega_c^2 + \omega^2} \tag{8}$$

where  $\omega_c$  is the cut-off frequency.

Figure 8. Bode-plot of ideal PR controller;  $K_p = 1$ ,  $K_i = 20$ ,  $\omega = 377$  rad/s, and  $\omega_c = 10$  rad/s.



Assuming  $\omega_c \ll \omega$ , equation (8) can be written as:

$$G_{PR\_non}(s) = K_{PR\_p} + K_{PR\_i} \frac{\omega_c s}{s^2 + 2\omega_c s + \omega^2} \quad (9)$$

The non-ideal PR controller gains are set by a reasonably high finite gain for eliminating the steady-state error. Substituting  $s = \frac{2}{T_s} \frac{1-z^{-1}}{1+z^{-1}}$  (bilinear transformation) into (9) gives the discrete transfer function of the PR controller as:

$$G_{PR}(z) = \frac{n_0 + n_1 z^{-1} + n_2 z^{-2}}{1 + d_1 z^{-1} + d_2 z^{-2}} \quad (10)$$

where  $T_s$  is the sampling time and:

$$n_0 = \frac{(4 + 4T_s \omega_c + \omega_0^2 T_s^2) K_p + 4K_i T_s \omega_c}{4 + 4T_s \omega_c + \omega_0^2 T_s^2}; \quad n_1 = \frac{(-8 + 2\omega_0^2 T_s^2) K_p}{4 + 4T_s \omega_c + \omega_0^2 T_s^2};$$

$$n_2 = \frac{(4 - 4T_s \omega_c + \omega_0^2 T_s^2) K_p - 4K_i T_s \omega_c}{4 + 4T_s \omega_c + \omega_0^2 T_s^2}; \quad d_1 = \frac{-8 + 2\omega_0^2 T_s^2}{4 + 4T_s \omega_c + \omega_0^2 T_s^2}; \quad d_2 = \frac{4 - 4T_s \omega_c + \omega_0^2 T_s^2}{4 + 4T_s \omega_c + \omega_0^2 T_s^2}$$

The digital equation of the PR controller is:

$$y(k) = n_0 u(k) + n_1 u(k-1) + n_2 u(k-2) - d_1 y(k-1) - d_2 y(k-2) \quad (11)$$

### 3.2. Feed-forward Compensation

Since the PR controller acts on a very narrow band around its resonant frequency  $\omega$ , a harmonic compensator for low-order harmonics can be implemented without any adverse effect on the behavior of the current controller [1]. The harmonic reduction can also be included in the structure by cascading several generalized integrators tuned to resonate at the desired frequency  $\omega$ . The transfer function of the harmonic compensator is given by:

$$G_{HC}(s) = \sum K_{PR\_ih} \frac{s}{s^2 + (h\omega)^2} \quad (12)$$

where  $h$  denotes the harmonic order.

For the extraction of the second-order harmonic, the harmonic compensator should be designed as follows:

$$G_{HC}(s) = \sum K_{PR\_ih} \frac{s}{s^2 + (h\omega)^2} \Bigg|_{h=2} = K_{PR\_i2} \frac{s}{s^2 + (2\omega)^2} \quad (13)$$

The Bode plot of the PR controller for  $\omega$  set to 120 Hz is shown in Figure 9. It can be seen that, this controller can achieve a very high gain and a zero phase shift in a narrow frequency band ( $\omega = 2\pi f = 2\pi \times 120 \text{ rad/s} = 754 \text{ rad/s}$ ). The width of the frequency band depends on the integral gain constant  $K_{PR\_i2}$ . Thus, it can also be used as a digital filter in order to compensate for the harmonics. Figure 10 shows a block diagram of PR controller for harmonic compensation.

**Figure 9.** Bode-plot of PR controller tuned for 120 Hz;  $K_p = 1$ ,  $K_i = 20$ ,  $\omega = 754$  rad/s, and  $\omega_c = 10$  rad/s.

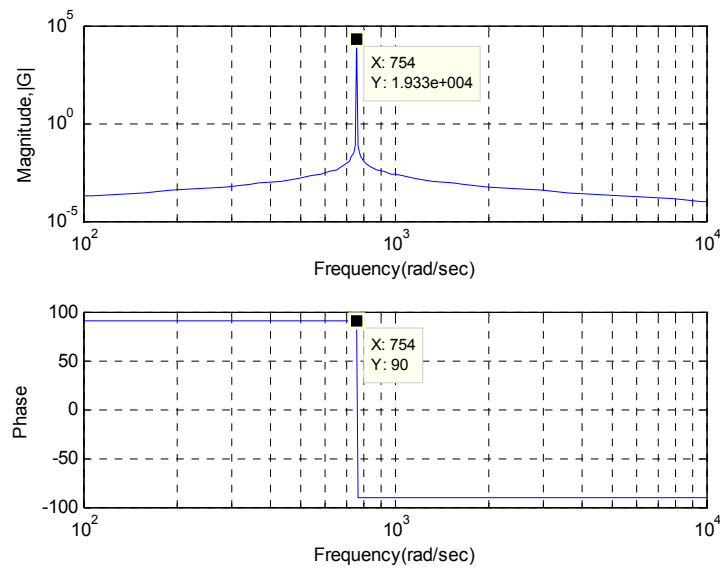
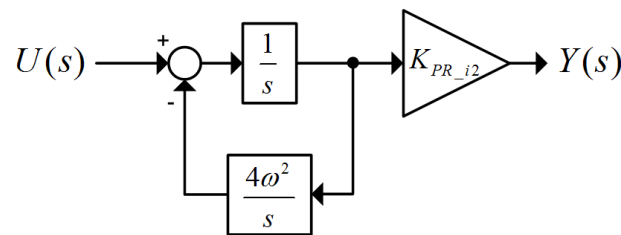
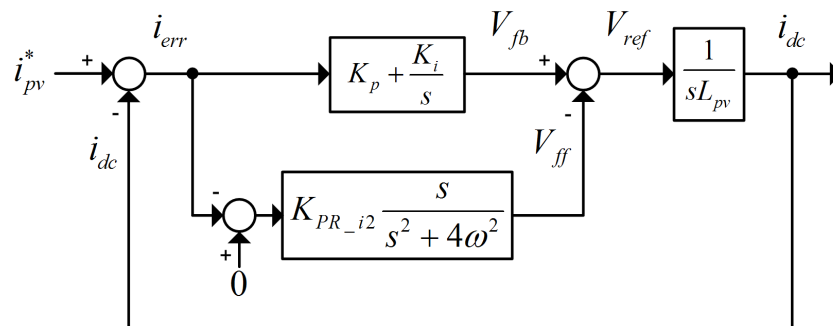


**Figure 10.** PR controller for harmonic compensation.



The second-order harmonic extracted from the PR controller can be used to compensate for the 120 Hz ripple. As shown in Figure 11, the extracted second-order harmonic is added to the output of the PI controller as a feed-forward component.

**Figure 11.** PI current controller with feed-forward compensation.



### 4. Simulation Results

The proposed algorithm was verified by performing a simulation using PSIM software as shown in Figure 12. The parameters used in the simulation are listed in Table 1.

**Figure 12.** Simulation diagram.

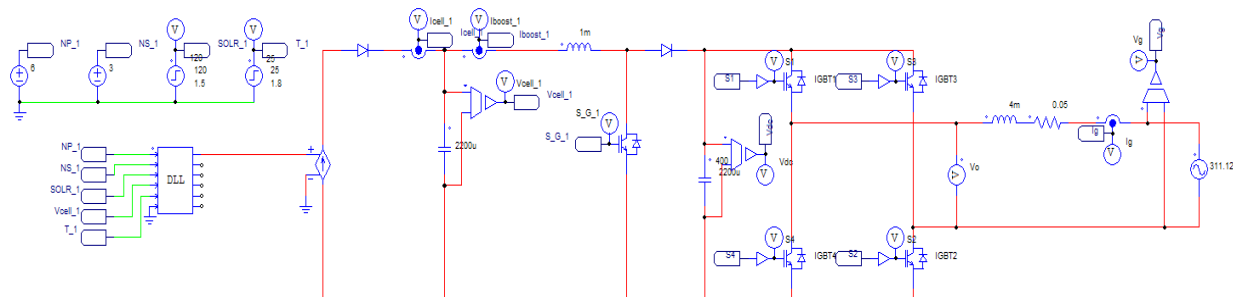


**Table 1.** Parameters of the simulation.

	Parameter	Value
Grid phase voltage	$E_{MAX}$	311.127 [V]
Grid frequency	$f$	60 [Hz]
Sampling period	$T_s$	100 [ $\mu$ s]
Grid-side inductor	$L_g$	4 [mH]
Grid-side resistor	$R_g$	0.05 [ $\Omega$ ]
Grid-side switch frequency	$f_{sw\_g}$	5 [kHz]
DC-link capacitor	$C_{dc}$	2,200 [ $\mu$ F]
PV-side inductor	$L_{pv}$	1 [mH]
PV-side capacitor	$C_{pv}$	2,200 [ $\mu$ F]
PV-side switch frequency	$f_{sw\_pv}$	5 [kHz]

Figure 13 shows the simulation waveform of the DC-link voltage. Under the influence of the second-order harmonic, the DC-link voltage is pulsating, as shown in Figure 13(a). It is found that the ripple component in the frequency domain represents the second-order harmonic as shown in Figure 13(b).

**Figure 13.** Simulation waveform of DC-link voltage. (a) Time domain; (b) frequency domain.

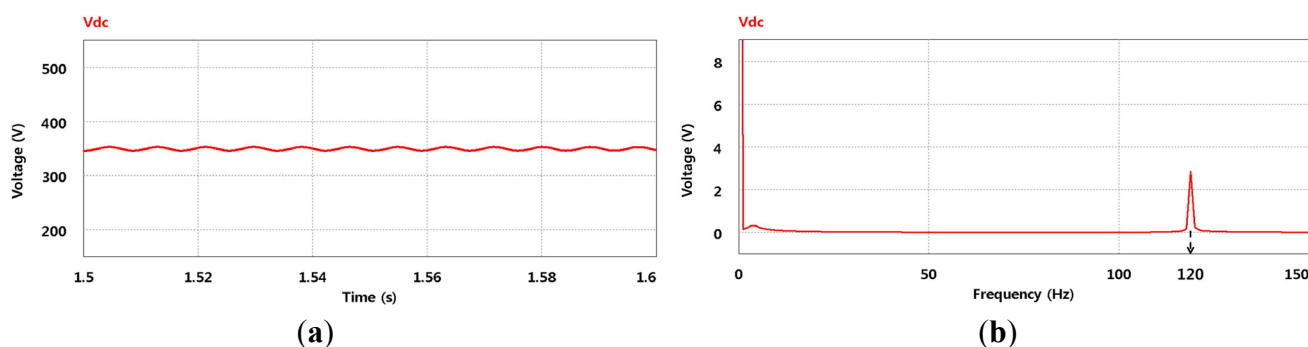
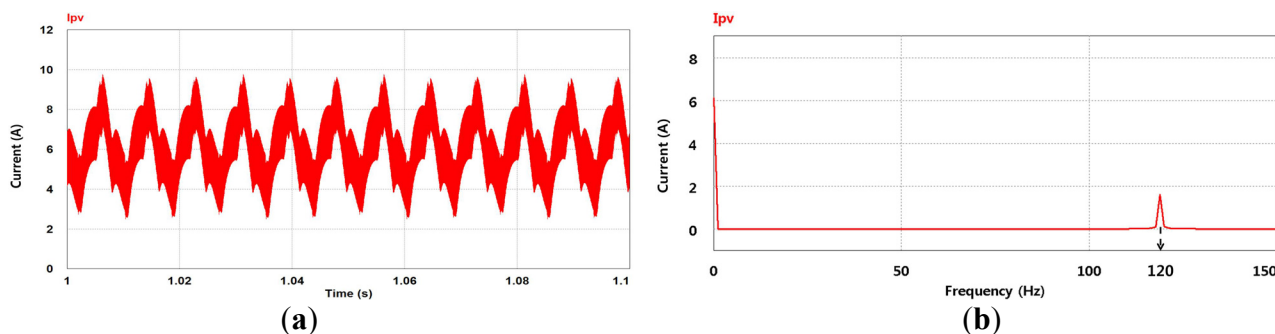


Figure 14 shows the simulation waveform of the PV current without compensation. The PV current is pulsating with the DC-link voltage, as shown in Figure 14(a). The second-order harmonic can be seen in the frequency domain, as shown in Figure 14(b).

**Figure 14.** Simulation waveform of PV current without compensation. (a) Time domain; (b) frequency domain.



The extracted second-order harmonic component using the PR controller is shown in Figure 15. As seen from this figure, the harmonic component can be extracted accurately. The extracted component is used to mitigate the second-order harmonic in the PV current.

**Figure 15.** Simulation waveform of the second-order harmonic component. (a) Time domain; (b) frequency domain.

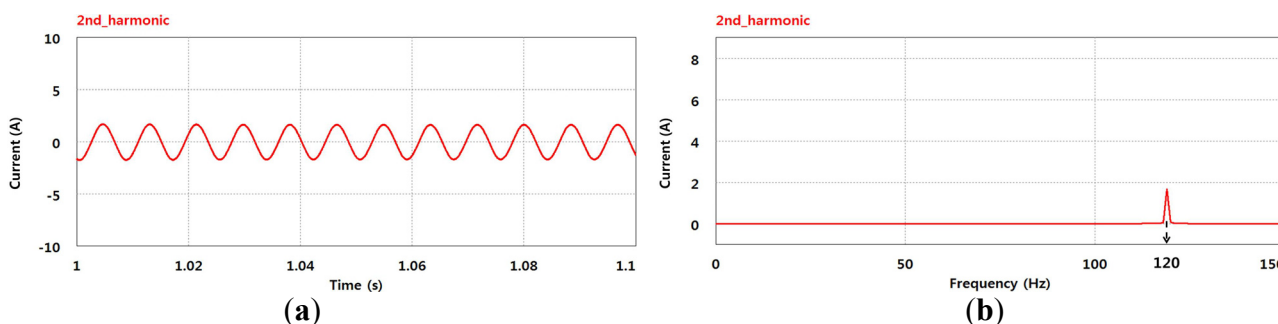


Figure 16 shows the simulation waveform of the PV current with compensation. It shows that the current ripples are reduced. Therefore, the effectiveness of the second-order harmonic reduction with the proposed feed-forward compensation is verified.

**Figure 16.** Simulation waveform of PV current with compensation. (a) Time domain; (b) frequency domain.

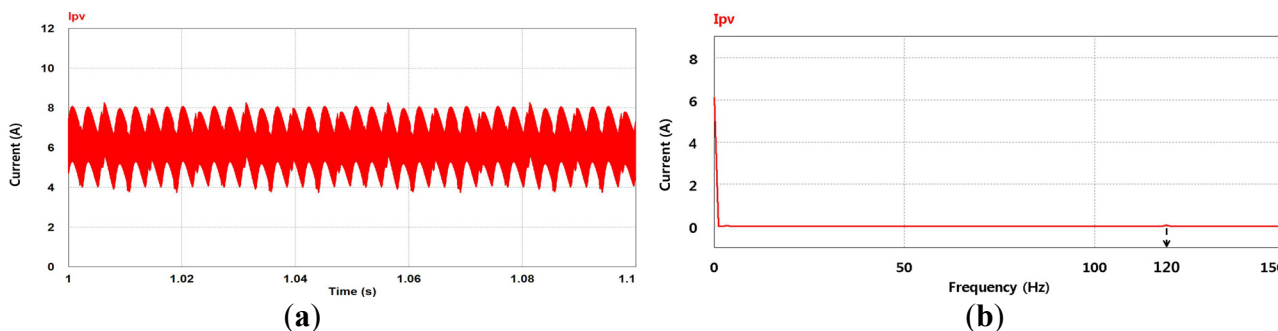


Figure 17 shows the simulation FFT waveform of the PV current before and after the harmonic compensation. In Figure 17, the switching frequency is 5 kHz. It can be seen that only the second-order harmonic have been compensated.

**Figure 17.** Simulation FFT waveform of PV current. (a) Without compensation; (b) with compensation.

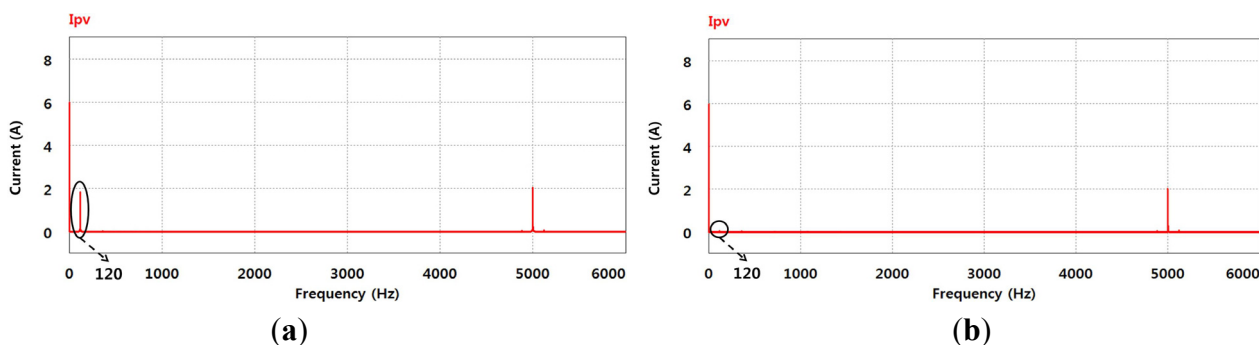
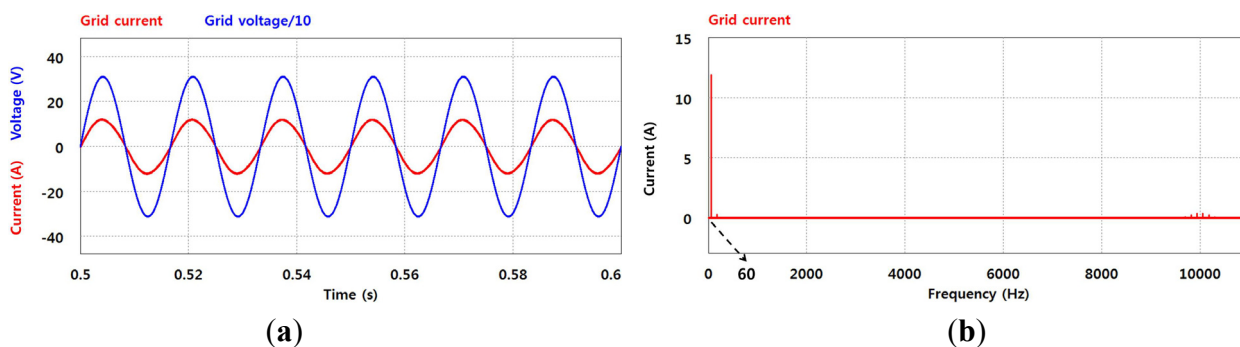
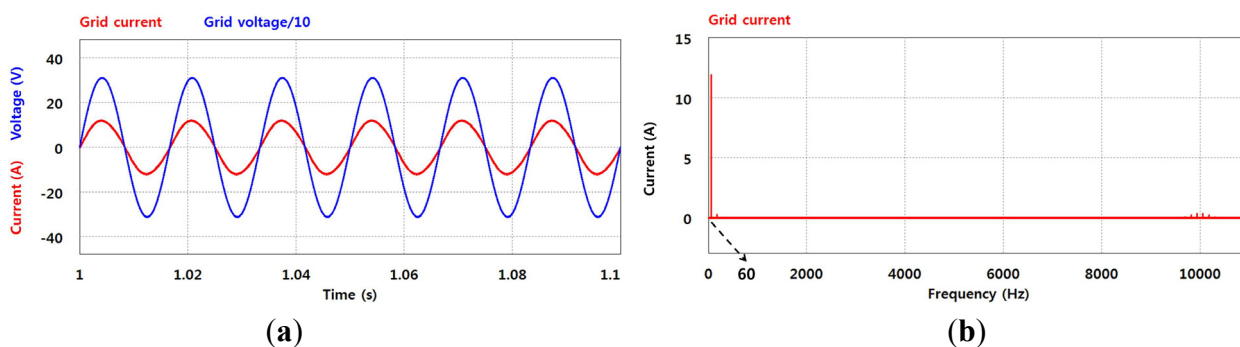


Figure 18 and Figure 19 show the simulation waveform of the grid current and voltage before and after the compensation. It shows that a proposed algorithm does not any bad effect on the grid current and voltage. Due to the large capacitance of the DC-link capacitor, the proposed algorithm does not affect the grid-side. As seen from these figures, the current controller is performed for unity power factor.

**Figure 18.** Simulation waveform of the grid current and voltage without compensation. (a) Time domain; (b) frequency domain.



**Figure 19.** Simulation waveform of the grid current and voltage with compensation. (a) Time domain; (b) frequency domain.



### 5. Experimental Results

The experiments were implemented on a PV PCS as shown in Figure 20. The proposed method was programmed on a TMS320F28335 digital signal processor (DSP). The experimental parameters were the same as the simulation values.

**Figure 20.** Experimental set.

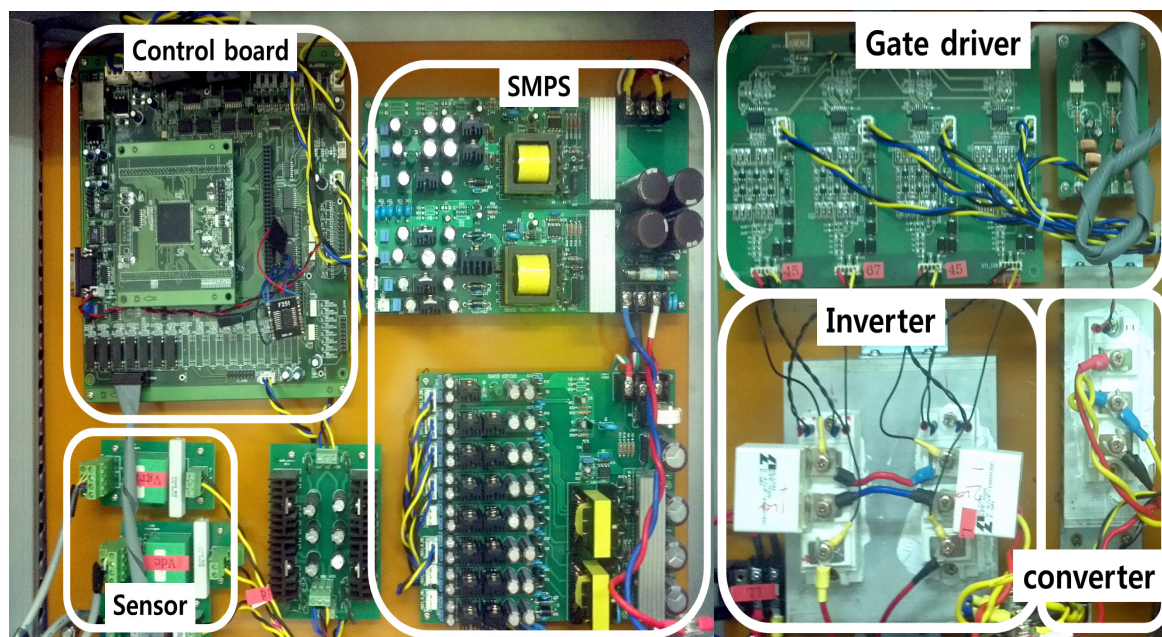
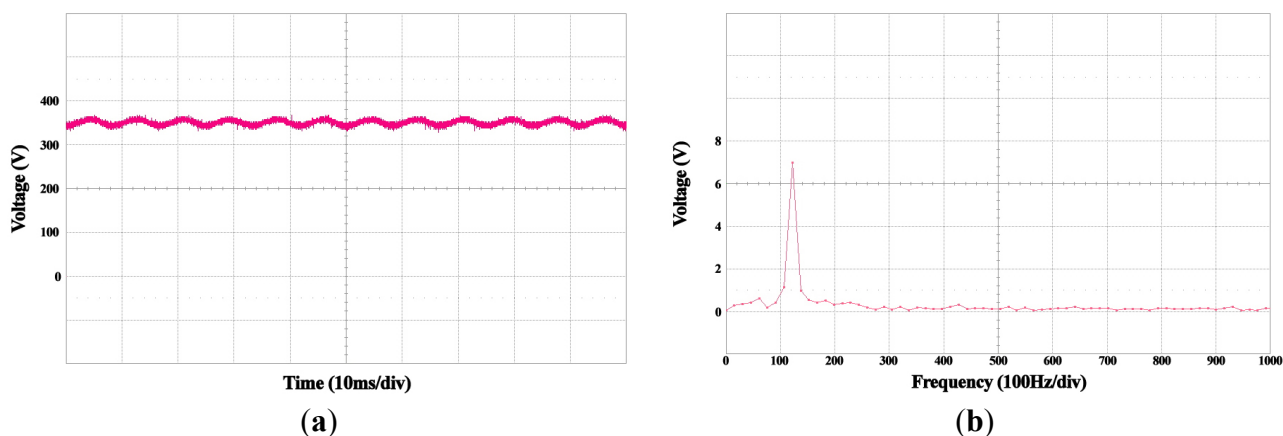


Figure 21 shows the experimental waveform with the DC-link voltage. Figure 21(a) shows the ripple of the DC-link voltage. Figure 21(b) shows the magnitude of the 120 Hz component of the DC-link voltage. It is seen that a ripple component with a magnitude of approximately 7 V is included.

**Figure 21.** Magnitude of DC-link voltage. (a) Time domain; (b) frequency domain.



Because of the ripple component, the PV current is pulsating as shown in Figure 22. The PV current is 6 A with  $\pm 0.95$  A (15.8%) current variation. To compensate for the ripple component, the PR controller extracts the second-order harmonic component from the PV current. Figure 23 shows the extracted component is exactly 120 Hz.

**Figure 22.** Magnitude of PV current without compensation. (a) Time domain; (b) frequency domain.

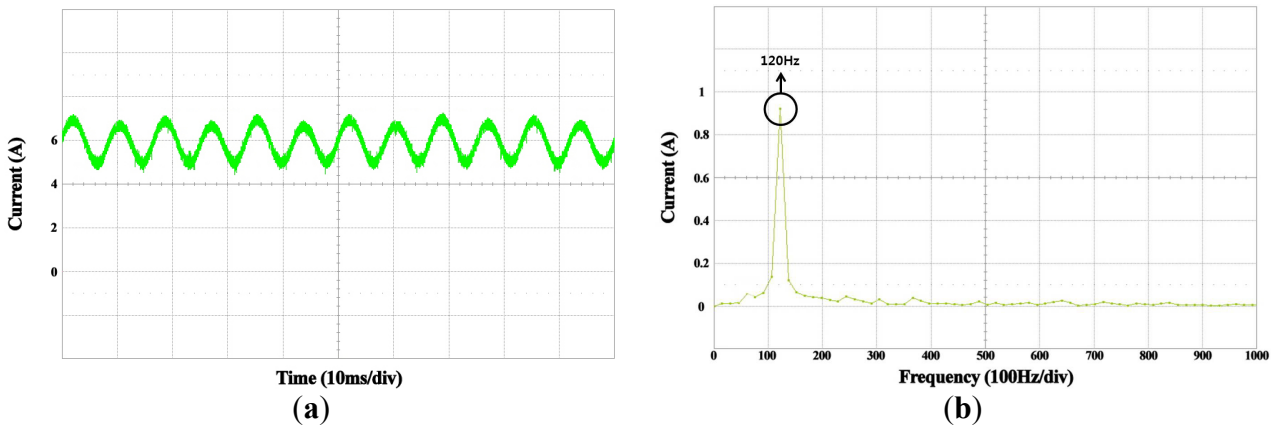


**Figure 23.** Magnitude of the second-order harmonic component. (a) Time domain; (b) frequency domain.

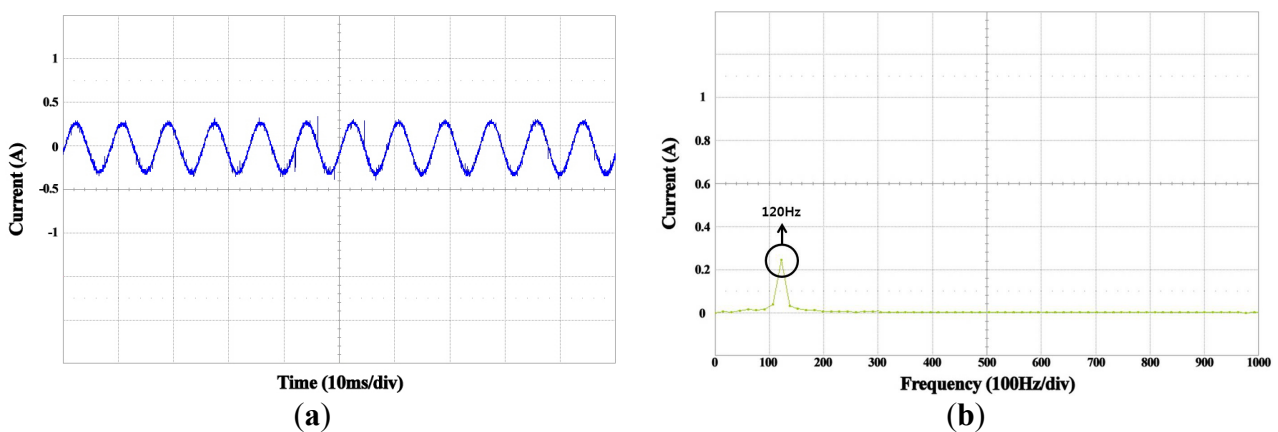
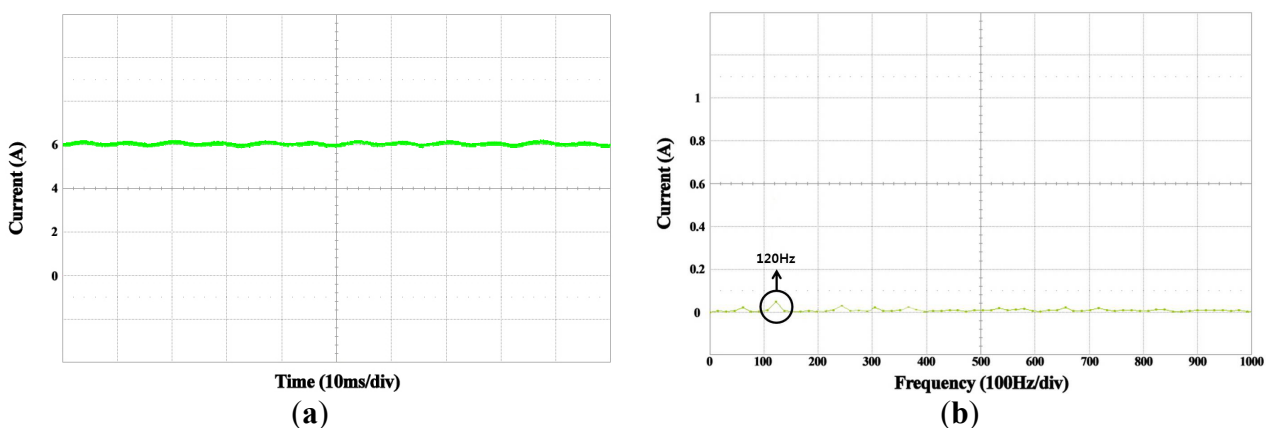


Figure 24 shows the result of the proposed feed-forward compensation using the PR controller. In Figure 24(a), the PV current seems to be composed of only the DC component. The PV current is 6 A with  $\pm 0.05$  A (0.008%) current variation. Figure 24(b) shows that the second-order harmonic is almost removed in the frequency domain.

**Figure 24.** Magnitude of PV current with compensation. (a) Time domain; (b) frequency domain.



In order to verify the proposed algorithm, MPPT control is performed using the PV simulator. Figure 25(a) shows the operating points of the PV array before the compensation. The power, current, and voltage of the PV array are observed to be changing continuously owing to the ripple component, as shown in Figure 25(b). After the proposed algorithm is applied, the operating points are fixed around the MPP, as shown in Figure 26(a). As can be seen in Figure 26(b), the power, current, and voltage are almost constant even after compensation.

**Figure 25.** Operating points of PV array before compensation. (a) P-V and I-V curve; (b) real-time plot.

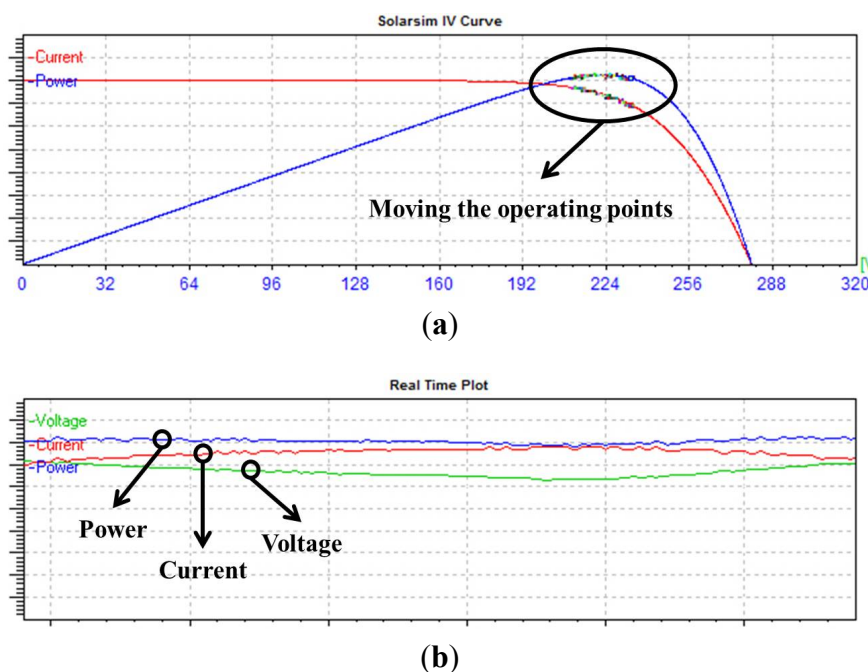


**Figure 26.** Operating points of PV array after compensation. (a) P-V and I-V curve; (b) real-time plot.

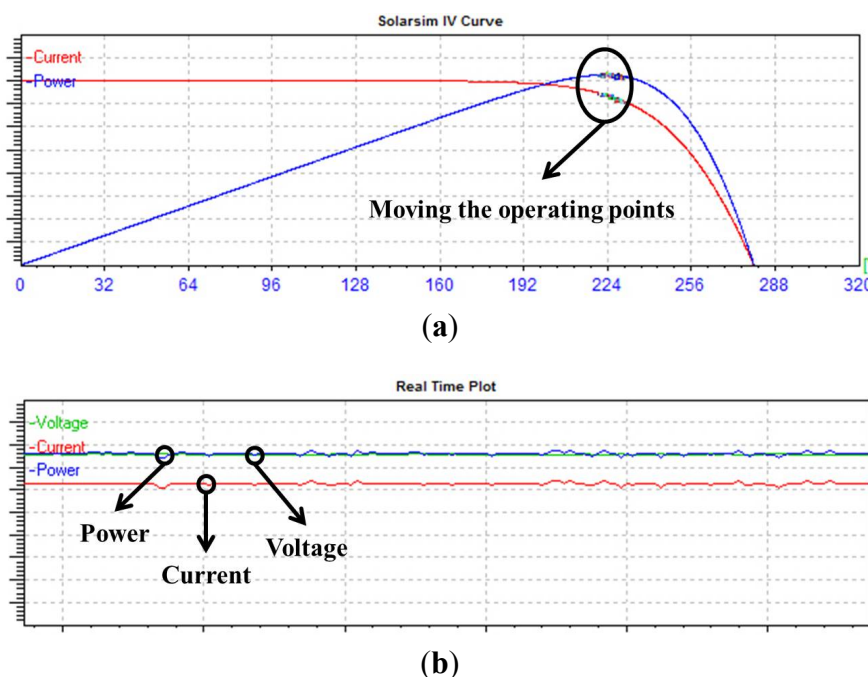


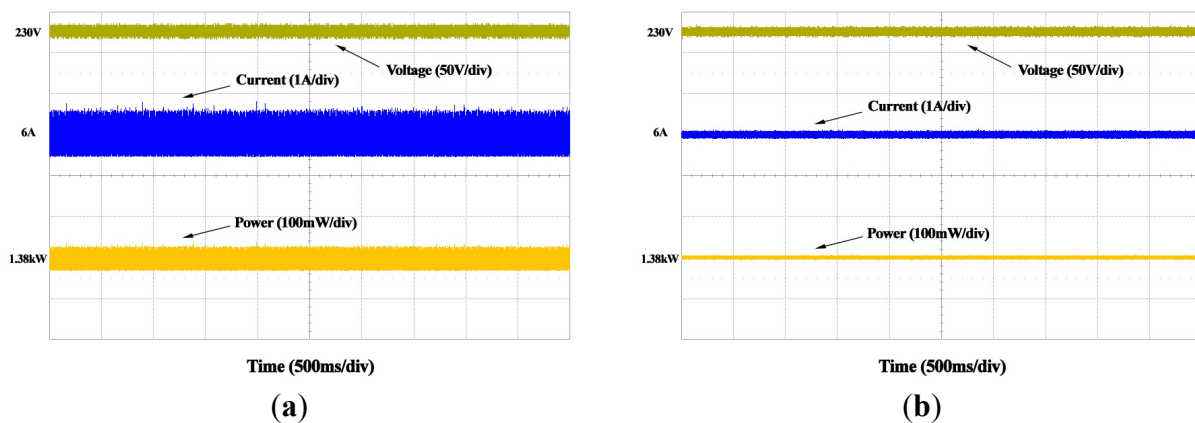
Figure 27 shows the PV voltage, current, and power during the MPPT control. As seen from Figure 27(a), the second-order harmonic component in the PV current is pulsating with the PV power as the ripple component. In Figure 27(a), the ripple of PV power is 70 W. The MPPT efficiency is:

$$95\% \approx \frac{1380 \text{ W} - 70 \text{ W}}{1380 \text{ W}} \times 100 \quad (14)$$

In Figure 27(b), the ripple of PV power is 20W after compensation. The MPPT efficiency is:

$$98.5\% \approx \frac{1380 \text{ W} - 20 \text{ W}}{1380 \text{ W}} \times 100 \quad (15)$$

**Figure 27.** Magnitude of a PV voltage, current, and power. (a) Without compensation; (b) with compensation.



## 6. Conclusions

This paper has proposed a second-order harmonic reduction technique using a PR controller for a PV PCS. It is possible to compensate for the 120 Hz ripple component of the PV current by using feed-forward compensation. The proposed second-order harmonic reduction technique is inexpensive and is easily implemented because additional devices or complex calculations are not required. The MPPT control works well after the proposed algorithm applied. The simulation and experimental results confirm the feasibility and effectiveness of the proposed algorithm.

## Acknowledgments

This work was supported by KETEP (20111020400030-11-1-000) which is funded by MKE (Ministry of Knowledge Economy) and by the Human Resources Development of the Korea Institute of Energy Technology Evaluation and Planning (KETEP) grant funded by the Korea government Ministry of Knowledge Economy (No. 20114010203030).

## References

1. Timbus, A.; Liserre, M.; Teodorescu, R.; Rodriguez, P.; Blaabjerg, F. Evaluation of current controllers for distributed power generation systems. *IEEE Trans. Power Electron.* **2009**, *24*, 654–664.

2. *IEEE Std 519-1992—IEEE Recommended Practices and Requirements for Harmonic Control in Electrical Power Systems*. IEEE: NY, USA, 9 April 1993.
3. *Electromagnetic Compatibility (EMC)—Part 3-2: Limits—Limits for Harmonic Current Emissions. IEC 61000-3-2*. International Electrotechnical Commission: Geneva, Switzerland, 23 March 1995.
4. Uyyuru, K.R.; Mishra, M.K.; Ghosh, A. An optimization-based algorithm for shunt active filter under distorted supply voltages. *IEEE Trans. Power Electron.* **2009**, *24*, 1223–1232.
5. Pawar, N.; Patidar, R.D.; Patidar, L.C. An Optimal Controller for Apf for Customer Harmonics and Reactive Power Compensation. In *Proceedings of IEEE Student Conference on Engineering and Systems (SCES)*, Uttar Pradesh, India, 16–18 March 2012; pp. 1–6.
6. Hamad, M.S.; Ahmed, K.H.; Williams, B.W. Selective Harmonic Filtering of a Medium Voltage Six-pulse Line Commutated Rectifier using an Adaptive Active Power Filter. In *Proceedings of 37th Annual Conference of the IEEE Industrial Electronics Society—IECON 2011*, Melbourne, Australia, 7–10 November 2011; pp. 943–948.
7. Safaee, A.; Yazdani, D.; Bakhshai, A.; Jain, P. A Three-Phase Adaptive Harmonic Extraction Approach for Active Power Filters. In *Proceedings of IEEE Applied Power Electronics Conference and Exposition*, Fort Worth, TX, USA, 6–10 March 2011; pp. 960–964.
8. Lee, S.H.; An, T.P.; Cha, H.J. Mitigation of low frequency ac ripple in single-phase photovoltaic power conditioning systems. *J. Power Electron.* **2010**, *10*, 328–333.
9. Liu, C.; Lai, J.S. Low frequency current ripple reduction technique with active control in a fuel cell power system with inverter load. *IEEE Trans. Power Electron.* **2007**, *22*, 1429–1436.
10. Gabe, I.; Montagner, V.; Pinheiro, H. Design and implementation of a robust current controller for VSI connected to the grid through an LCL filter. *IEEE Trans. Power Electron.* **2009**, *24*, 1444–1452.
11. Alajmi, B.N.; Ahmed, K.H.; Finney, S.J.; Williams, B.W. Fuzzy-logic-control approach of a modified hill-climbing method for maximum power point in microgrid standalone photovoltaic system. *IEEE Trans. Power Electron.* **2011**, *26*, 1022–1030.
12. Jeong, H.G.; Roh, H.S.; Lee, K.B. An improved maximum power point tracking method for wind power systems. *Energies* **2012**, *5*, 1339–1354.
13. Schenck, M.E.; Lai, J.S.; Stanton, K. Fuel Cell and Power Conditioning System Interactions. In *Proceedings of IEEE Applied Power Electronics Conference and Exposition*, Austin, TX, USA, 6–10 March 2005; pp. 114–120.
14. Dang, P.; Petzoldt, J. A New Control Method for Eliminating the 2nd Harmonic at the DC link of a Shunt APF under an Unbalanced and Nonlinear Load. In *Proceedings of Power Electronics and Applications*, Birmingham, UK, 30 August–1 September 2011; pp. 1–5.
15. Rodriguez, P.; Luna, A.; Munoz-Aguilar, R.; Etxeberria-Otadui, I.; Teodorescu, R.; Blaabjerg, F. A stationary reference frame grid synchronization system for three-phase grid-connected power converters under adverse grid conditions. *IEEE Trans. Power Electron.* **2011**, *27*, 99–112.
16. Ahmed, K.H.; Massoud, A.M.; Finney, S.J.; Williams, B.W. A modified stationary reference frame based predictive current control with zero steady-state error for LCL coupled inverter-based distributed generation systems. *IEEE Trans. Power Electron.* **2011**, *58*, 1359–1370.
17. Yang, S.; Lei, Q.; Peng, F.Z.; Qian, Z. A robust control scheme for grid-connected voltage source inverters. *IEEE Trans. Power Electron.* **2011**, *58*, 202–212.

18. Rodriguez, P.; Luna, A.; Candela, I.; Mujal, R.; Teodorescu, R.; Blaabjerg, F. Multiresonant frequency-locked loop for grid synchronization of power converters under distorted grid conditions. *IEEE Trans. Power Electron.* **2011**, *58*, 127–138.
19. Sun, J.; Chen, B.; Guo, S.; Zha, X.; Xiong, L.; Gong, J. High-Reliability and Harmonic-Sharing Dual Parallel Topology for Active Power Filter. In *Proceedings of IEEE Power Electronics for Distributed Generation Systems*, Hefei, China, 16–18 June 2010; pp. 240–245.

© 2013 by the authors; licensee MDPI, Basel, Switzerland. This article is an open access article distributed under the terms and conditions of the Creative Commons Attribution license (<http://creativecommons.org/licenses/by/3.0/>).